Wireless Personal Communications (2020) 112:651–673
https://doi.org/10.1007/s11277-020-07066-y

A Crest Factor Reduction Scheme with Optimum Spacing Peak Cancellation for Intra-band Non-contiguous Carrier Aggregated OFDM Signals

Pooria Varahram[1] · Somayeh Mohammady[1] · Ronan Farrell[1] · John Dooley[1]

Published online: 18 January 2020

Abstract
This paper proposes a new crest factor reduction scheme to reduce instantaneous-to-average power ratio (IAR) resulting decent peak reduction, and adjacent channel leakage ratio (ACLR) reduction, though the error vector magnitude (EVM) is significantly enhanced. In the conventional peak cancellation (CPC) technique, peak regrowth occurs as a result of finite impulse response (FIR) filter windows overlapping. The peak regrowth problem in CPC technique can be compensated, though this will lead to increased computational complexity and degradation in EVM. The proposed algorithm allocates spacing to contiguous peaks to avoid FIR filter windows overlapping. Two types of overlapping are discussed, incremental and decremental. The optimum spacing can be determined from the FIR filter impulse response characteristic. Simulations are carried out with different intra-band non-contiguous carrier aggregated OFDM signals. The results of simulations show between 3 and 10% improvement in EVM performance while maintaining equivalent IAR and ACLR performance. Applying the proposed optimum spacing peak cancellation scheme compared to the conventional peak cancellation technique.

Keywords Crest factor reduction (CFR) · Power amplifier · Peak cancellation · Peak regrowth

✉ Somayeh Mohammady
somayeh.mohammady@tudublin.ie; somayeh.mohammady@mu.ie

Pooria Varahram
p_varahram@yahoo.com; pooria.varahram@mu.ie

Ronan Farrell
Ronan.Farrell@mu.ie

John Dooley
john.dooley@mu.ie

[1] National University of Ireland, Maynooth, Ireland

1 Introduction

Envelope variation of the signal caused by high data rate, can give rise to high signal peaks. This problem is known as high peak to average power ratio (PAPR). When these peaks in the signal pass through the power amplifier they give rise to adjacent channel interference that in turn can violate the spectrum emission mask (SEM) [1]. To avoid this, the signal power delivered to the power amplifier may be backed off. However, while this can lead to linear performance, it causes power efficiency degradation resulting in poor coverage in a cellular system, call interruptions and lower quality of service. Hence, a solution to reduce PAPR is imperative. CFR techniques are referred as PAPR reduction techniques. Both CF and PAPR are expressed in decibels and here they are assumed to be equivalent. However it should be noted that CF is the square root of PAPR, $PAPR = CF^2$. There are different scenarios of carrier aggregated (CA) OFDM signals, intra-band contiguous CA, inter-band CA and intra-band non-contiguous CA [2]. This paper studies the latter case which has wider range of envelope deviation compared to the contiguous CA and hence more advanced CFR techniques are required to deal with this type of signal. To date, many CFR techniques have been developed in communication systems. In general, these techniques can be categorized as either distortion-based such as clipping and filtering [3], peak windowing (PW) [4], noise shaping (NS) [5] and conventional peak cancellation (CPC) [6] or distortion-less such as partial transmit sequence (PTS) [7] and selected mapping (SLM) [8]. The other way to categorize the CFR techniques is based on their location in the system. Most of the techniques are located prior to digital up-conversion (DUC). While operating at a lower sample rate has a benefit of lowering the performance requirements of the hardware, due to carrier aggregation in DUC, lower performance may be achieved. It is important to mention that choosing a CFR technique depends on the application and traffic in the channel. For example, in the case of single carrier signal, scrambling techniques [7, 8] are a good choice, but for the multi-carrier signals, as a result of carriers combining at the up conversion stage, a CFR technique should follow the DUC unit.

The CPC is the most promising technique in terms of complexity and performance among the clipping techniques. This is due to the fact that only selected peaks pass through the filter which significantly reduces the complexity. Moreover, there is no additional hardware at the receiver. Despite these features, the main problem with CPC is peak regrowth. The peak regrowth occurs due to the FIR filter windows overlapping. By passing the scaling signal of detected peaks through the FIR filter, the overlapping between samples occurs as a result of high level main lobe and side lobes in the FIR filter impulse response. The peak regrowth problem causes spectral leakage which can violate the SEM and increases the standard deviation of the clipping noise that deteriorates the error vector magnitude (EVM) performance. As a result of the peak regrowth problem, the CPC technique requires 2 or more stages which significantly increases the complexity and thus it may not be efficient for some multi-carrier applications [9].

In [10], a parabolic peak cancellation (PPC) technique is proposed in OFDM systems. To achieve the targeted CFR performance, at least 3 stages of PPC are required; however no analysis of clipping noise and EVM performance has been reported. In [11], a CFR technique is proposed for dual-band systems. Authors report EVM as the main problem of CPC and hence they separately apply it for each band. But this architecture requires several stages of PC for each band, as also reported in [10]. In [12], a CFR technique is proposed, which is based on clipping and filtering for inter-band carrier aggregation signals. A similar architecture is presented as the technique in [11]. Even though the implementation

of this technique is at a lower frequency, which requires a lower number of filter taps, it requires more hardware resources compared to the CPC technique.

In this paper, a new CFR scheme is proposed in order to avoid FIR filter windows overlapping and to enhance the overall system performance. The proposed solution is to apply spacing determined from the FIR filter impulse response to the contiguous peaks in order to eliminate the peak regrowth and suppress the clipping noise distortion. Different algorithms to determine the required spacing for each stage are provided. The obtained spacing values are then tested to evaluate overall performance. By applying the optimum spacing values to the contiguous peaks prior to filtering, the optimum peaks will be selected. The proposed scheme is validated through simulations with different non-contiguous CA signals.

The rest of the paper is organized as follows. Section 2 presents some description of the system and reviews the CPC technique. In Sect. 3, first, the FIR filter design is presented and then the issue of FIR filter window overlapping is discussed. The proposed optimum spacing peak cancellation (OSPC) algorithm is subsequently introduced. Sections 4 and 5 discuss the simulation results and present the conclusion, respectively.

2 System Description

In this section, first, an intra-band non-contiguous CA–OFDM system is described and the conventional peak cancellation technique is reviewed.

2.1 Intra-band Non-contiguous Carrier Aggregated OFDM

Figure 1 shows the block diagram of a transmitter in a wireless communication system. The CFR block is located following the DUC unit.

From this figure, each baseband signal denotes $\tilde{x}_n^{(1)}$ and $\tilde{x}_n^{(2)}$ is up-converted by DUC unit first, and then its aggregation will be transferred to the CFR block. The aggregated signal can be expressed by,

$$\begin{aligned} x_n &= x_n^{(1)} + x_n^{(2)} \\ &= Re\left(\tilde{x}_n^{(1)} \exp(j\omega_1 Ln) + \tilde{x}_n^{(2)} \exp(j\omega_2 Ln)\right) \end{aligned} \tag{1}$$

where $x_n^{(1)}$ and $x_n^{(2)}$ are the up-converted carrier components (CCs), $\tilde{x}_n^{(1)}$ and $\tilde{x}_n^{(2)}$ are the baseband envelope signals and L is the oversampling factor.

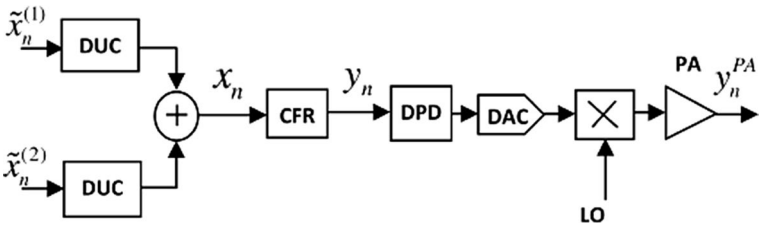

Fig. 1 Block diagram of an intra-band non-contiguous CA–OFDM system with CFR

The DUC block comprises of interpolation filtering, mixing, combining and fractional re-sampling. In this way, several combinations of carriers can be achieved. Even though the placement of CFR after DUC deals with a wideband signal which requires a higher number of filter taps, this architecture guarantees the overall performance requirement. The carrier combinations create some peaks after the DUC, which the CFR applied prior to DUC, is would not be able to compensate for [2]. The data stream after the CFR is transferred to digital predistortion (DPD) followed by digital to analog converter (DAC), a local oscillator (LO) mixer, a power amplifier (PA) and will be transmitted.

2.2 Conventional Peak Cancellation

Figure 2 shows the block diagram of the CPC technique.

In this instance, the magnitude and phase components of the input signal are first generated and then the complex peak scaling signal is obtained as,

$$c_n = \begin{cases} 0 & \text{if} \quad |x_n| \le A_{th} \\ ((|x_n| - A_{th})e^{i\theta_n}) & \text{if} \quad |x_n| > A_{th} \end{cases} \tag{2}$$

where A_{th} is a predefined threshold which can be selected based on the specific requirements of a particular communication standard or the operation of the system hardware and $|x_n|$ and θ are the magnitude and phase of the input signal, respectively. At the same time, detected peaks (i.e. the peaks above the threshold) obtained from the magnitude of the input signal, generates a peak indicator pulse (PIP). Each PIP gets the amplitude of the peaks and creates the scaling pulse by multiplying by the peak phase and passing through a filter. The output signal after applying an FIR filter is then as follows,

$$\begin{aligned} y_n &= x_n - \sum_{p=1}^{N_p} \left(\left| x_{n_p} - A_{th} \right| \delta_{n-n_p} e^{j\theta_{n_p}} \right) * h_k \\ &= x_n - \sum_{p=1}^{N_p} \left| x_{n_p} - A_{th} \right| h_{n-n_p} e^{j\theta_{n_p}} \\ &= x_n - \sum_{p=1}^{N_p} c_{n_p} h_{n-n_p} \end{aligned} \tag{3}$$

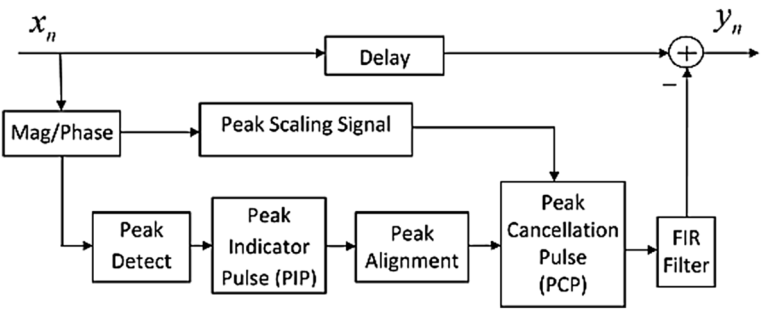

Fig. 2 Block diagram of the CPC technique

where the sign * denotes the convolution, h_k is an FIR filter impulse response centered at $k_c=(K+1)/2$, c_{np} is the complex peak scaling signal at sample n_p, $|x_{np}|$ and θ_{np} are the magnitude and phase of the selected peak, respectively. It should be noted that δ_n is the spacing after nth stage, and the index N_p denotes the number of detected peaks. It is also important to note that the value of N_p is not fixed and it depends on the number of detected peaks which is not predictable. It also depends on several parameters such as the number of carriers, carrier configuration and the modulation scheme used.

In the peak alignment block, the peak indicator pulses are delay adjusted. The output of the PIP is transferred to a block called peak cancellation pulse (PCP). The PCP is a complex peak scaling signal obtained from (2) and aligned at the location of the PIP. Each PCP is occupied for the duration of the filter length and the coming peaks shall wait until the process of the running PCP is completed. Finally, all the PCPs are accumulated and subtracted from the delayed input signal. It should be noted that the number of PCPs at each clock cycle are limited in hardware in order to improve the efficiency. In this paper, it is assumed that the number of PCPs allocated for all the analysis in the simulations is maximized. While CPC achieves high performance, its main limitation as reported in [9] is it may not be efficient for multi-carrier applications. This is because of the requirement of several stages of CPC for multi-carrier signals which significantly increases the complexity. In the next section, a new CFR scheme is proposed which achieves the required performance for CA–OFDM signals with only two stages.

3 Optimum Spacing Peak Cancellation Scheme

The block diagram of the proposed PC scheme is shown in Fig. 3. It can be seen that in the proposed scheme, optimum spacing identification and optimum peak placement blocks are included following the peak detection.

The reason for applying the spacing to the detected peaks is to avoid FIR filter overlap. The optimum spacing is identified from the FIR filter impulse response. The algorithm to obtain the spacing is introduced in the following section. In order to describe the OSPC scheme, first, an FIR filter is designed and its characteristic is analyzed.

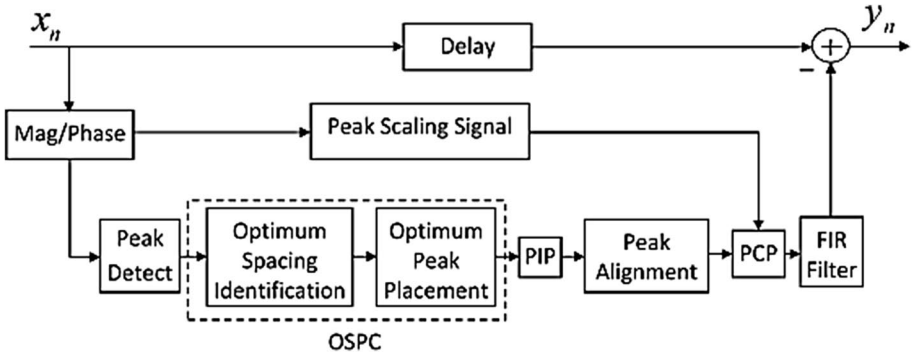

Fig. 3 Block diagram of the proposed OSPC scheme

3.1 FIR Filter Design

To explain the optimum spacing identification algorithm, the FIR filter impulse response has to be obtained. This can be done by recalling the coefficients that are stored in the system memory. For each standard, the corresponding filter can be designed offline and its coefficients are stored in memory. Due to the fact that the CFR depends on the traffic in the channel, the CFR requirement can vary over time. Hence, the filter characteristic which is based on the input signal changes accordingly. One of the main aspects of the proposed OSPC scheme is that the optimum spacing can be identified online and hence can be adapted to suit the system specifications. The convolution operation in (3) can be represented as a filter structure. But the impulse response of an ideal filter will be non-causal and infinite which is not practically feasible. Hence a truncation is required to limit the length of the filter.

The FIR filter can be any window function. In this paper, a Kaiser window is used due to its low level of side lobes to suppress the out-of-band (OOB) radiation and adjustable parameters. Moreover, the Kaiser window is optimal in the sense of the concentration of its peak around center frequency [13]. The Kaiser window weights, W_k can be defined as,

$$W_k = \begin{cases} \dfrac{I_0\left(\pi\alpha\sqrt{1-\left(1-\frac{2k}{K-1}\right)^2}\right)}{I_0(\pi\alpha)} & 0 \le k \le K-1 \\ 0 & \text{otherwise} \end{cases} \tag{4}$$

where $I_0(.)$ is the zeroth order Bessel function, K is the filter length and is odd and α is a non-negative real number that determines the trade-off between the main lobe width and the side lobe level. This is an important parameter to design the filter which impacts on the filter windows overlapping and peak regrowth of the CPC technique. In this paper, the impulse response of the composite filter for multi-carrier signals denoted by h_k can be given by,

$$h_k = \sum_{r=1}^{M} W_k e^{2\pi j\left(k-\frac{K}{2}\right)\frac{f_r}{f_s}} \quad k = 0, 1, 2, \ldots, K-1 \tag{5}$$

where M is the number of carriers, f_r is the center frequency of the r_{th} carrier, f_s is the sampling frequency and W_k is the discrete impulse response of a single carrier filter. It should be noted that h_k for the multi-carrier signals not centered around the zero hertz is complex and for a single carrier signal is real.

3.2 FIR Filter Windows Overlapping

FIR filter window overlap is a major problem for the CPC technique and can cause peak regrowth. For the CPC technique, this can be solved by adding additional CPC stages. In doing this however the computational complexity is significantly increased, and it does not automatically guarantee the desired performance. In this subsection, the FIR filter window overlap is studied and it is shown that this problem does not always create peak regrowth. The proposed OSPC scheme offers better PAPR reduction and EVM performance without additional complexity or latency as compared to CPC. This is due to the addition of optimum spacing to the contiguous peaks. This is achieved by keeping the FIR filter settings

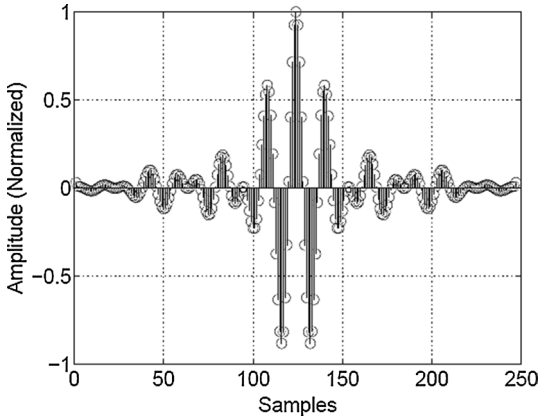

Fig. 4 FIR filter impulse response for two CA signal

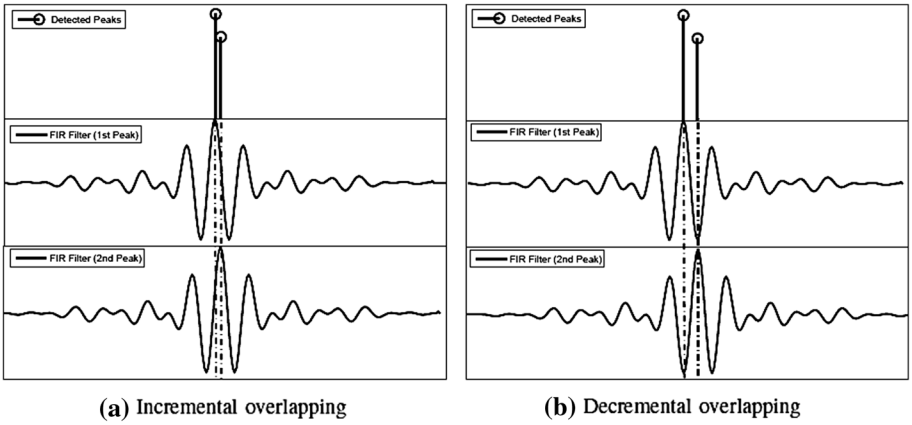

(a) Incremental overlapping **(b)** Decremental overlapping

Fig. 5 FIR filter window overlapping scenarios, **a** incremental overlapping, **b** decremental overlapping

the same with the same number of taps. Since the latency depends on the filter length and corresponding number of taps, in the proposed scheme the filter does not change. The complexity also depends on the number of stages, and in the proposed scheme is the same as for CPC. Figure 4 shows the FIR filter impulse response for two CA signals designed by (5).

It can be observed that the FIR filter has a main lobe at the center and two strong side lobes at either side. These side lobes are a result of mixing two single carrier filters. In the CPC technique, the PCPs following the filter will be overlapped. The overlapping can be categorized to incremental and decremental as shown in Fig. 5. It is also possible that the incremental and decremental overlapping occurs at further side lobes. But these side lobes are often negligible due to their low level. Moreover, considering those side lobes cause CFR performance degradation or non-ideal complementary cumulative distribution function (CCDF) performance due to canceling several peaks. Hence, in the proposed scheme only the main lobe and the first side lobe with the highest amplitude are considered. In both scenarios in Fig. 5, peak regrowth occurs, however, the peak regrowth is only created when A_{th} is low. For high values of A_{th}, there will be no peak regrowth, however, overlapping causes clipping noise distortion.

The other possibility that causes peak regrowth is when one peak is detected while the other peak has an amplitude near A_{th}. The peak regrowth problem can be overcome by additional stages of the CPC technique at the expense of clipping noise distortion and EVM performance degradation. Here, the clipping noise is discussed in more detail. The clipping noise at instant n can be defined as,

$$e_n = x_n - \beta y_n \tag{6}$$

where the scaling parameter β is obtained by performing a least-squares fit between the CFR input and output signals as below,

$$\beta = \frac{E\{|x_n|^2\}}{E\{\tilde{x}_n y_n\}} \tag{7}$$

where $\tilde{x}_n$ is the complex conjugate of the input signal x_n. As demonstrated in [14], the value of β for CA–OFDM is approximately one. Hence, the inverse of β is also one, and A_{th} does not have any effect on it. While the primary objective is to reduce the PAPR of the signal, the in-band distortion and OOB radiation should simultaneously not be compromised. The impact of the former is evaluated using EVM and the latter is measured by adjacent channel leakage ratio (ACLR). The CPC technique does not cause OOB radiation, while the PAPR reduction performance is maintained. A reduction in PAPR can be achieved with the CPC technique, but this comes at the expense of clipping noise distortion [15]. In [16], the clipping noise is derived for OFDM systems. It is shown that due to the correlation of samples in the main lobe, one peak canceling in the parabolic pulse is enough for peak detection in OFDM systems. However, for non-contiguous carrier aggregation signals, there are several short pulses in one period of the signal, hence overlapping can often occur. Moreover, the samples of the signal used in this paper are not independent and identically distributed (i.i.d.) and are correlated.

In this paper, the main objective however is to minimize the cost function of the clipping noise or the mean-square-error in (6) which is given by,

$$\xi_n = E\{|e_n|^2\}. \tag{8}$$

In the next section, it will be shown that minimizing ξ_n enhances the EVM performance. By replacing (3) in (6), and single stage of CPC, the clipping noise can be given by,

$$e_n = x_n - \left(x_n - \sum_{p=1}^{N_p} c_{n_p} h_{n-n_p} \right). \tag{9}$$

Equation (9) can be simplified to,

$$e_n = \sum_{p=1}^{N_p} c_{n_p} h_{n-n_p}. \tag{10}$$

Equation (10) shows that the clipping noise is a series of filtered pulses. Now consider two contiguous PCPs with the spacing of δ ($n_{i+1}=n_i+\delta$), then (10) can be rewritten as,

$$e_n = c_{n_i} h_{n-n_i} + c_{n_{i+1}} h_{n-n_{i+1}} \tag{11}$$

where c_{n_i} and $c_{n_{i+1}}$ are the PCPs at peak locations of n_i and n_{i+1}, respectively. In (11), the optimum spacing that causes no overlapping to PCPs is $\delta \geq K/2$. The optimum spacing is the value that gives best overall performance of the system. However, overlapping is inevitable, as several peaks are detected in period of K_2 samples. In the incremental overlapping scenario, the value of δ is in the range of $1 \leq \delta \leq 4$, and in the decremental overlapping $5 \leq \delta \leq 12$. It can be assumed that the amplitude of PCP at sample n_{i+1} is μ times the amplitude of PCP at sample n_i, i.e. $\left|c_{n_{i+1}}\right| = \mu \left|c_{n_i}\right|$ and $0 \leq \mu \leq 1$. From the triangular inequality of the complex numbers, the instantaneous power of the clipping noise in (11) can be obtained by,

$$\begin{aligned} |e_n|^2 &= \left|c_{n_i} h_{n-n_i} + c_{n_{i+1}} h_{n-n_{i+1}}\right|^2 \\ &\leq \left(\left|c_{n_i} h_{n-n_i}\right| + \left|c_{n_{i+1}} h_{n-n_{i+1}}\right|\right)^2 \end{aligned} \tag{12}$$

To compare the clipping noise power for both overlapping scenarios, (12) can be simplified to,

$$\begin{aligned} |e_n|^2 &\leq \left(\left|c_{n_i} h_{n-n_i}\right| + \left|c_{n_{i+1}} h_{n-n_{i+1}}\right|\right)^2 \\ &\leq \left(\left|c_{n_i}\right|\left|h_{n-n_i}\right| + \left|c_{n_{i+1}}\right|\left|h_{n-n_{i+1}}\right|\right)^2 \\ &\leq \left(\left|c_{n_i}\right|\left|h_{n-n_i}\right| + \mu\left|c_{n_i}\right|\left|h_{n-n_{i+1}}\right|\right)^2 \\ &\leq \left|c_{n_i}\right|^2 \left(\left|h_{n-n_i}\right| + \mu\left|h_{n-n_{i+1}}\right|\right)^2. \end{aligned} \tag{13}$$

In (13), $\left|c_{n_i}\right|^2$ is a constant. From (13), the clipping noise power depends only on the superposition of the absolute values of the FIR filter impulse responses. Now the cost function which is the mean of the clipping noise power in (13) can be given by,

$$\begin{aligned} \xi_n &= E\left\{\left|c_{n_i}\right|^2 \left(\left|h_{n-n_i}\right| + \mu\left|h_{n-n_{i+1}}\right|\right)^2\right\} \\ &= \left|c_{n_i}\right|^2 E\left\{\left(\left|h_{n-n_i}\right|^2 + \mu^2\left|h_{n-n_{i+1}}\right|^2 + 2\mu\left|h_{n-n_i}\right|\left|h_{n-n_{i+1}}\right|\right)\right\}. \end{aligned} \tag{14}$$

Due to the linearity property of the expected value operator, (14) can be simplified to,

$$\xi_n = \left|c_{n_i}\right|^2 E\left\{\left|h_{n-n_i}\right|^2 + \mu^2 E\left|h_{n-n_{i+1}}\right|^2 + 2\mu E\left(\left|h_{n-n_i}\right|\left|h_{n-n_{i+1}}\right|\right)\right\}. \tag{15}$$

From [17], as covariance between two random variables can be defined as the expected product of their deviations from their individual expected values, (15) can be rewritten as:

$$\xi_n = \left|c_{n_i}\right|^2 \left\{E\left|h_{n-n_i}\right|^2 + \mu^2 E\left|h_{n-n_{i+1}}\right|^2 + 2\mu E\left|h_{n-n_i}\right| E\left|h_{n-n_{i+1}}\right| + 2\mu \mathrm{Cov}\left(\left|h_{n-n_i}\right|, \left|h_{n-n_{i+1}}\right|\right)\right\}, \tag{16}$$

where Cov stands for covariance. From (16), an important conclusion can be made. For both overlapping scenarios in Fig. 5, FIR filter impulse responses $\left|h_{n-n_i}\right|$ and $\left|h_{n-n_{i+1}}\right|$ are correlated. However, in the no overlapping case, i.e. $\delta \geq K/2$, the two signals are pairwise

uncorrelated which makes the covariance in (16) zero. In (16), the expected value terms $E\left|h_{n-n_i}\right|^2$, $E\left|h_{n-n_{i+1}}\right|^2$ and $E\left|h_{n-n_i}\right| E\left|h_{n-n_{i+1}}\right|$ are positive and the same for both overlapping scenarios. Moreover, the covariance in (16) is non-negative, i.e. $\mathrm{Cov}\left(\left|h_{n-n_i}\right|, \left|h_{n-n_{i+1}}\right|\right) \geq 0$. Then, the cost function ξ_n is greater than the case where there is no overlapping. Generally, reducing the spacing between contiguous peaks, increases the covariance in (16) that leads to an increase in ξ_n. This is due to the higher side lobe levels near the center tap of the FIR filter. It is noted that, by increasing μ, the cost function ξ_n will be increased. But, there is no control over the value of μ, as the detected peaks have random magnitudes. Hence, to achieve the objective in (8), the overlapping must be minimized. In eliminating the main lobe and the first side lobe, a spacing is allocated to the contiguous peaks. This required spacing according to the filter designed in Fig. 4, must be 4 and 12, respectively. The spacing should be chosen judiciously as high spacing causes loss of some peaks that results in non-ideal CCDF performance. The cost function in (8) can be generalized for all the detected peaks N_p in (10) and the same objective can be achieved. In the case of CPC with two stages and after simplification in (10), the clipping noise can be written as,

$$e_n = \sum_{p=1}^{N_p} c_{n_p} h_{n-n_p} + \sum_{p=1}^{N_p'} c'_{n_p} h_{n-n_p} \tag{17}$$

where and N_p' are the PCPs and the number of detected peaks at the second stage, respectively. It is expected that the number of peaks at the second stage is less than the first stage, i.e. $N_p' < N_p$. By repeating (12)–(16), it can be proven that the cost function of the clipping noise in (8) for two stages of CPC becomes lower by increasing the spacing between the two contiguous peaks. The algorithm to obtain these spacing values for each stage is now provided.

3.3 Optimum Spacing Identification Algorithm

In this subsection, two algorithms to identify the spacing at each stage of CPC are introduced. To do that, the first step is to locate the FIR filter center tap denoted k_c where $k_c = (K+1)/2$. Intuitively at this point, the filter has its maximum amplitude. Next, the filter should be normalized. This is done by dividing $|h_k|$ by the maximum of its absolute value, $\hat{h}_k = \frac{|h_k|}{\max\{|h_k|\}}$. The reason of absolute value of h_k is due to the complex values of h_k. Hence the normalized amplitude of the center tap becomes $\hat{h}_{k_c} = 1$. It should be noted that due to the symmetry of the FIR filter, only one side of the filter needs to be selected to search for the optimum spacing values.

The other consideration is that, the filter coefficients, h_k are scaled values due to fixed point operation in hardware. Hence the normalization is only to identify the optimum spacing values. The sample sequence of FIR filter impulse response can be given by,

$$sample(k) = \left\{1, 2, \ldots, \frac{K+1}{2}, \frac{K+1}{2} + 1, \ldots, K\right\} \tag{18}$$

and due to the symmetry of the FIR filter,

$$h_k = h_{K-k+1}, \quad 1 \leq k \leq \frac{K+1}{2} - 1. \tag{19}$$

According to this algorithm, a search for the number of samples between the center tap and the second zero crossing in the FIR filter impulse response is performed. A threshold parameter denoted as η can be defined to eliminate some small peaks in the FIR filter impulse response. The value of η depends on some factors such as sampling rate and the number of carriers. In this paper, $\eta=0$ which is referred to as zero crossing. However, higher values of η can be defined if the performance achievement does not violate the standard requirement. This is because in the CFR technique, some distortion (i.e. below the spectral emission mask) can be tolerated. In summary, the OSPC algorithm can be expressed as follows,

Algorithm 1 OSPC Algorithm for the First Stage

1: **Initialization**
- set $i = 0$
- set the value of $\eta = 0$
- set number of searching to $L = \frac{K+1}{2} - 1$

2: Load FIR filter coefficients and save it to h_k
3: Find the length of the FIR filter K =length(h)
4: Normalize the FIR filter impulse response and find its absolute $\hat{h}_k = \frac{|h_k|}{\max(|h_k|)}$
5: Locate the FIR filter center tap $k_c = \frac{K+1}{2}$
6: Locate the second highest peak (in the case of two stages) in the FIR filter impulse response, $\left|\hat{h}_{k_p}\right|$
7: **for** $i \leq L$ **do**
8: **if** $\hat{h}_{k_p+i} \geq \eta$ **then**
9: $i = i + 1$
10: **else**
11: save the distance between the location of the peak and the center tap $\delta_1 = k_p - k_c + i$
12: break
13: **end if**
14: **end for**

The other optimum spacing value for the second stage can be obtained from Algorithm 2 as follows,

Algorithm 2 OSPC Algorithm for the Second Stage

1: **Initialization**
- set $i = 0$
- set the value of $\eta = 0$
- set number of searching to $L = \frac{K+1}{2} - 1$

2: Load FIR filter coefficients and save it as h_k
3: Find the length of the FIR filter K =length(h)
4: Normalize the FIR filter impulse response and find its absolute $\hat{h}_k = \frac{|h_k|}{\max(|h_k|)}$
5: Locate the FIR filter center tap $k_c = \frac{K+1}{2}$
6: Locate the highest peak in the FIR filter impulse response (i.e. the FIR filter coefficients) $\hat{h}_{k_c}$
7: **for** $i \leq L$ **do**
8: **if** $\hat{h}_{k_c+i} \geq \eta$ **then**
9: $i = i + 1$
10: **else**
11: save the optimum spacing value $\delta_2 = i$
12: break
13: **end if**
14: **end for**

To achieve the required performance mandated by the 3GPP wireless standard [1], more than one stage is required. The second optimum spacing is calculated based on the number of samples from the center tap to the first zero crossing. It should be noted that the lower the spacing value, the higher the probability of the peak regrowth and the higher the spacing value, the higher the probability of missing some peaks. Therefore, it is crucial to identify zero crossing points. Algorithm 1 is capable of operating for more than two stages, and as a result, third or higher order peaks in the FIR impulse response can be obtained at step 6 of the algorithm. This is due to the fact that higher spacing at the first stage, eliminates both side lobe and main lobe samples. The process of searching for the optimum spacing values can be done online or offline. The main benefit of online search for optimum spacing is in adaptability of the system for different input signals. As the optimum spacing values can vary for different signal standards, the algorithm adaptability is very beneficial.

4 Numerical Analysis

To evaluate the performance of the OSPC scheme, two signals have been applied. First, a two CA signal with 5 MHz bandwidth for each carrier and 15 MHz separation from the center of the carrier with 122.88 Mbps sample rate and second, a three CA signal with 5 MHz bandwidth for each carrier and 15 MHz separation between carriers and sampling frequency of 122.88 Mbps. The clipping ratio (CR) is defined as the ratio of the clipping threshold A_{th} to the standard deviation of the input signal in dB, $\gamma = 20 \log (A_{th}/\sigma_x)$. The value of γ also indicates the target CFR. The parameter α for the Kaiser

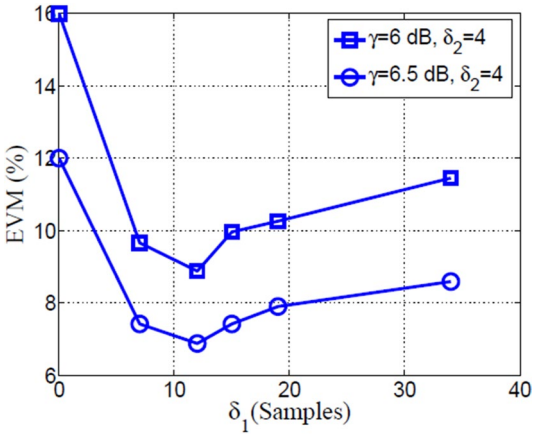

Fig. 6 EVM reduction performance for two CA signal

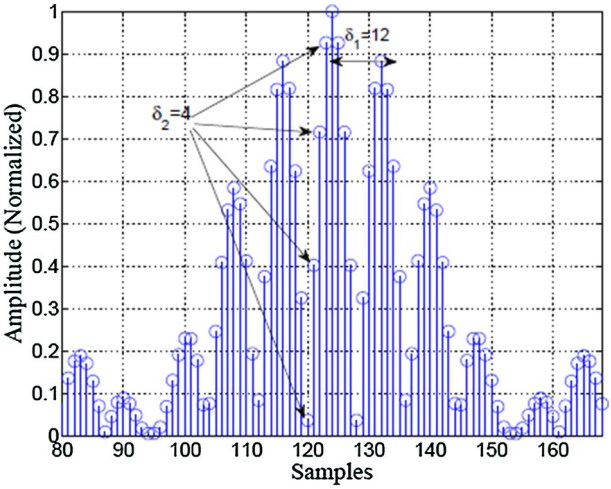

Fig. 7 FIR filter impulse response magnitude for two carrier signal

filter is $\alpha = 1.6$ and the filter tap length $K = 247$. These parameters have to be chosen carefully to achieve the required OOB suppression and maintain adequate EVM and CFR performance. By applying an OSPC algorithm from Sect. 3, the optimum spacing values for each of these signals can be obtained.

Figures 6 and 7 show the magnitude of the FIR filter impulse response for two and three carrier signals, respectively. From these figures, the optimum spacing values for two carrier and three carrier signals are $\delta_1 = 12$, $\delta_2 = 4$ and $\delta_1 = 10$, $\delta_2 = 3$, respectively. It can be observed that the side lobes level for the three carrier signal are lower than the two carrier signal. This means that the impact of the FIR filter on peak regrowth and clipping noise distortion is more significant in the case of the two carrier signal (Fig. 8).

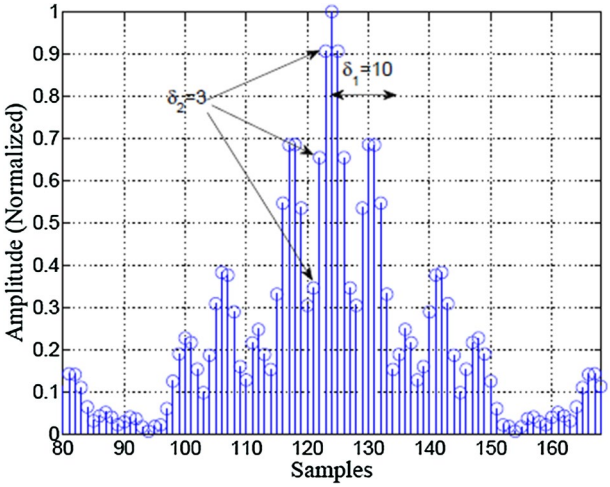

Fig. 8 FIR filter impulse response magnitude for three carrier signal

4.1 Instantaneous to Average Power Ratio (IAR) Analysis

It is crucial to ensure that the metric used for measuring the effectiveness of CFR has the minimum amount of uncertainty. While PAPR or also known as crest factor is the most popular metric used in the literature, it is important to note that in some cases in order to achieve higher power efficiency, some distortions below the spectral emissions mask for a particular communication standard can be tolerated. In other words, as PAPR or crest factor uses symbol by symbol calculation, some peaks will be overlooked in the data stream. An alternative metric to evaluate the performance of distortion-based techniques which looks at the peaks with higher accuracy is named instantaneous amplitude reduction (IAR) [18]. Figures 9 and 10 show the CCDF comparison between the OSPC scheme and CPC when $\gamma = 6$ and 7 dB for two and three carrier signals, respectively.

It can be seen that both techniques achieve comparable *IAR* reductions with 2 stages. However for the CPC technique, the desired *IAR* reduction achieves this performance at

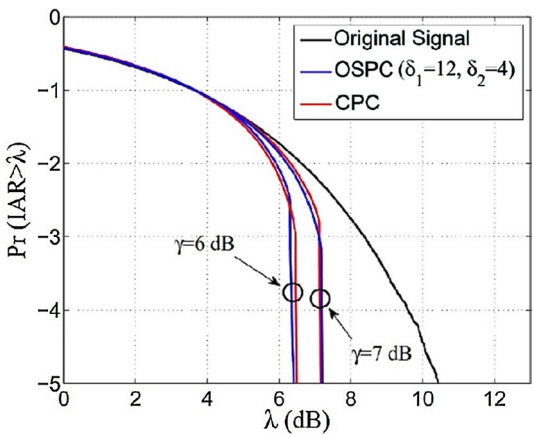

Fig. 9 CCDF comparison for two carrier signal for $\gamma = 6$ and 7

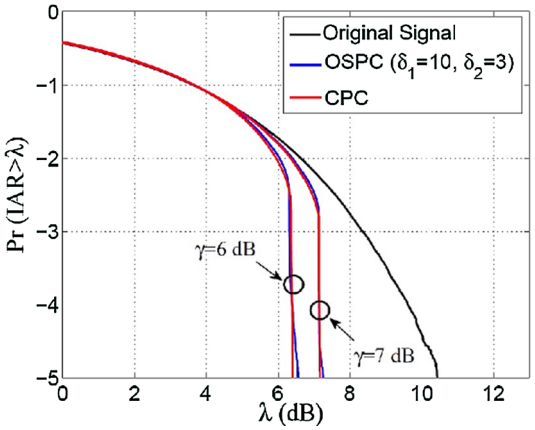

Fig. 10 CCDF comparison for three carrier signal for $\gamma = 6$ and 7

the expense of EVM degradation. This is due to the FIR filter windows overlapping in the CPC technique.

It is possible to improve the EVM performance for the CPC technique by increasing truncation order, but this comes at an increase in the complexity, with the need for more than 2 stages. In order to maintain the complexity of the system, two stages are recommended.

4.2 EVM Analysis

The error vector between the desired signal and the measured signal is defined as EVM. Mathematically, it is the square root of the ratio of the mean error vector power to the mean reference power. For multi-carrier signals, the composite EVM can be obtained by $EVM\,(\%) = 100 \cdot \sqrt{\frac{P_{err}}{P_{reference}}} = 100 \cdot \sqrt{\frac{E\left\{|e_n|^2\right\}}{E\left\{|x_n|^2\right\}}}$, P_{err} and $P_{reference}$ are the root mean square (RMS) power of the error and the reference signal, respectively [19]. From this definition, a single value of EVM will be obtained. The results of EVM versus *IAR* reduction (*dIAR* or *dPAPR*) for different techniques are shown in Figs. 10 and 11, respectively. Additional CCDF result is illustrated by Fig. 14 in order to analyze the performance of OSPC technique with verity of γ.

It can be observed that the OSPC scheme with $\delta_1 = 12$ and $\delta_2 = 4$ achieves the desired IAR reduction with significantly lower EVM performance. The enhancement for a three carrier signal is not as significant as for a two carrier signal. This is because of higher side lobes in the FIR filter impulse response of two carrier signal compared to that of the three carrier signal.

Figures 12 and 13 show the EVM performance by varying the first stage spacing δ_1 for two and three carrier signals, respectively.

It can be observed that at the spacing of $\delta_1 = 12$ for the two carrier signal, and $\delta_1 = 10$ for the three CA signal, the lowest EVM performance is achieved. As seen in Fig. 11, and Fig. 13, the minimum of the plots occurs when $\delta_1 = 12$, and $\delta_1 = 10$. This means that in order to have minimum EVM, optimum value of 10, and 12 must be assigned. This is also supported by the analytical derivation in the previous section.

It has been shown that the cost function ξ_n in (8) is minimized by eliminating the main and first side lobe by allocating the optimum spacing. It should be noted that

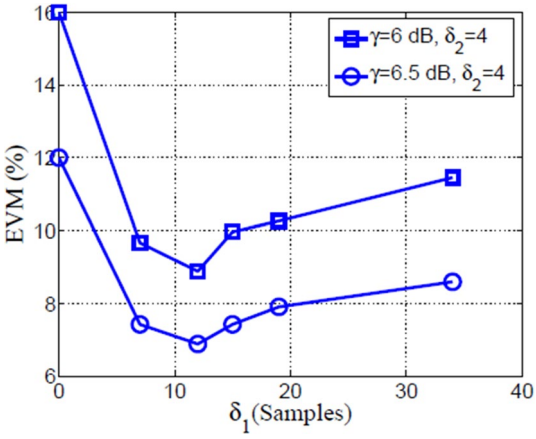

Fig. 11 EVM variation with sample spacing for two carrier signal

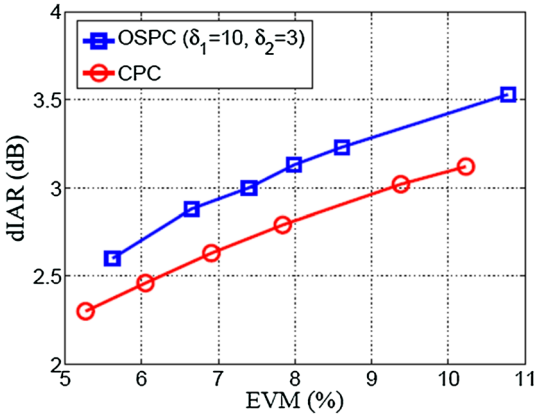

Fig. 12 EVM variation with sample spacing for three carrier signal

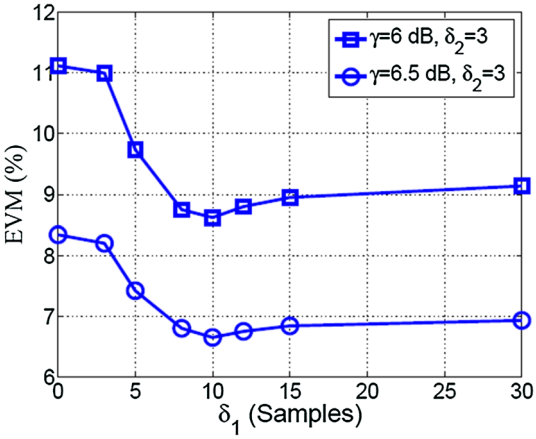

Fig. 13 EVM versus spacing for three carrier signal when $\delta_2 = 3$

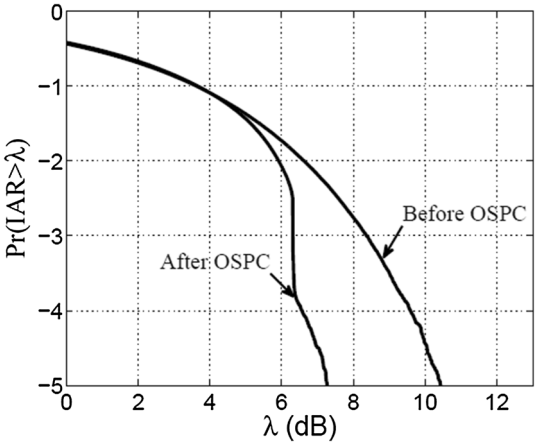

Fig. 14 Non-ideal CCDF curve for two carrier signal when $\delta_1 = \delta_2 = 12$

increasing the spacing does not necessarily enhance the EVM performance. This is due to the fact that higher spacing values (i.e. greater than the optimum spacing) leaves some peaks which degrades the EVM performance. It should be noted that the spacing values obtained from Algorithm 2 are optimum due to the fact that higher values give non-ideal CCDF curve as shown in Fig. 14.

From this figure, the CCDF curve is non-ideal for the proposed OSPC scheme when $\delta_1 = \delta_2 = 12$. The ideal CCDF curve is a straight line down, in contrast to the non-ideal curve in which the curve veers outwards to higher *IAR* regions. This shows that choosing a high spacing value leaves some peaks in the data stream which is reflected in the CCDF result (Figs. 14 and 15).

Hence, to compensate that, more stages will be required and as a result, the complexity and latency will be increased. The non-ideal CCDF curve also causes problem for the digital pre-distortion block following CFR. To show the effectiveness of the OSPC scheme, an analysis has been performed for different γ values. This is important as the *IAR* reduction requirements could vary. This depends on the traffic in the channel and cell coverage which requires the power amplifier to transmit at its higher power.

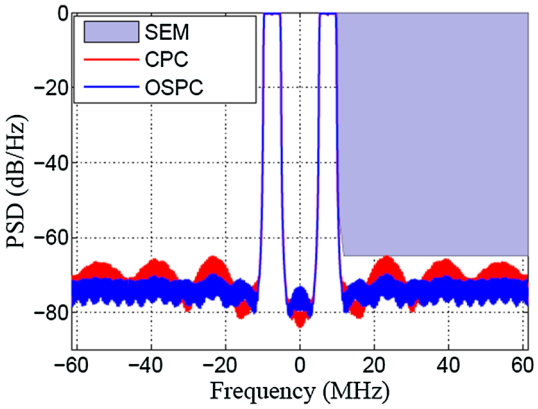

Fig. 15 PSD Comparison for two CA signal when $\gamma = 6$ dB

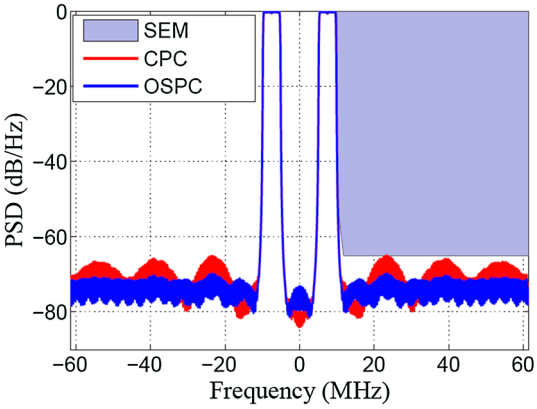

Fig. 16 PSD Comparison for two CA signal when $\gamma = 6$ dB

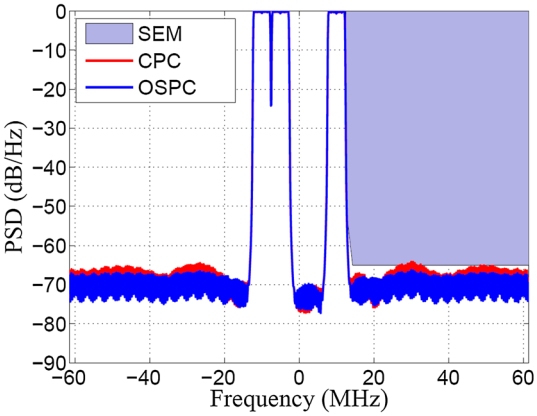

Fig. 17 PSD Comparison for three CA signal when $\gamma = 6$ dB

4.3 ACLR Analysis

The ACLR is defined as the ratio of the total power over the channel bandwidth to the power delivered in the adjacent channels (both upper sideband-US, and lower sideband-LS). The ACLR for each band is calculated from $ACLR[dBr] = \left(\int_B P_{out}(f)df\right) / \left(\int_{LS} P_{out}(f)df + \int_{US} P_{out}(f)df\right)$. The ACLR indicates the minimum adjacent power level in order to not interfere with the adjacent channels. Then, it is necessary to avoid the high level of OOB. Figures 16 and 17 show the normalized power spectral density (PSD) for the two and three carrier signals, respectively. It is shown that ACLR of both techniques is below the SEM mandated by the 3GPP standard [1]; however the OSPC scheme shows slightly better ACLR performance.

Figures 18 and 19 show the spectrum comparison of the clipping noise (ξ) between CPC and OSPC scheme for two and three CA signals, respectively. From these figures, the clipping noise distortion is higher for two CA signal compared to three CA signal. This is due to the high level side lobes in the FIR filter impulse response of the two CA signal. It can be observed that the proposed OSPC scheme achieves the lower clipping noise level compared to the CPC.

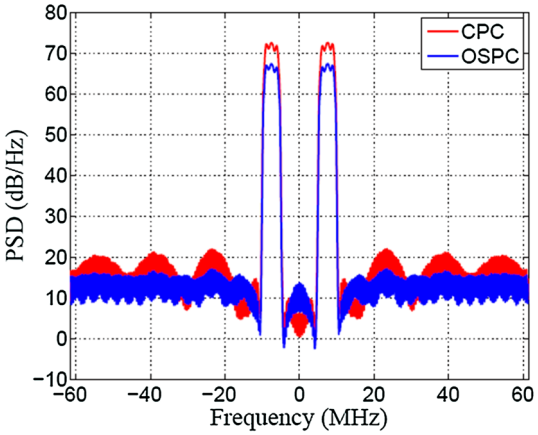

Fig. 18 Clipping noise comparison for two CA signal when γ = 6 dB

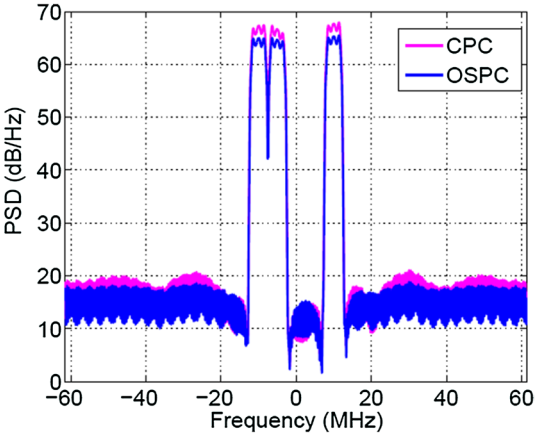

Fig. 19 Clipping noise comparison for three CA signal when γ = 6 dB

Table 1 Performance comparison of the CPC technique at different γ for two carrier signal

γ (dB)	IAR (dB) reduction at 0.01%	EVM (%)	ACLRl/ACLR2 (dBr)	CCDF at 0.1%	CCDF at 0.01%	CCDF at 0.001%
5.5	3.39	21.06	68.1/68.2	6.17	6.19	6.2
6	3.12	16.11	69.4/69.5	6.45	6.47	6.488
6.5	2.78	12.02	71.2/71.4	6.77	6.8	6.82
7	2.4	8.69	73.1/73.2	7.12	7.18	7.2

Table 2 Performance comparison of the OSPC scheme at different γ with $\delta_1 = 12$ and $\delta_2 = 4$ for two carrier signal

γ (dB)	IAR (dB) reduction at 0.01%	EVM (%)	ACLRI/ACLR2 (dBr)	CCDF at 0.1%	CCDF at 0.01%	CCDF at 0.001%
5.5	3.59	11.13	70.5/70.6	5.95	5.99	6.08
6	3.24	8.88	74.1/74.2	6.3	6.345	6.41
6.5	2.86	6.88	77.2/77.3	6.7	6.73	6.76
7	2.44	5.16	80.1/80.2	7.12	7.14	7.17

Tables 1 and 2 present the performance comparisons of the CPC and OSPC schemes for different γ values, respectively. From Table 1, the CPC achieves the target IAR reduction for γ of 5.5, 6, 6.5 and 7 with poor EVM performance. The ACLR1 and ACLR2 meet the performance requirement of 60 dB for all the values of γ. The results in Table 2 show significant EVM improvement by applying the OSPC scheme with comparable IAR reduction and the ACLR performance is almost marginally improved.

Tables 3 and 4 shows the performance comparison for the three carrier signal. A similar improvement is reported for this signal by applying the OSPC scheme. To ensure that the CCDF curve is ideal, it is measured at different probabilities; however the IAR reduction is measured at 0.01% probability according to the standard.

5 Conclusions

This paper proposes a new CFR scheme using OSPC algorithm. According to this scheme, a search for the number of samples between the filter center tap and the first sample with the amplitude less than a pre-defined threshold is performed. Following the identification of the optimum spacing values, the optimum peaks are selected. The selection of optimum peaks leads to significant enhancement in EVM performance with comparable IAR reduction and ACLR compared to the conventional peak cancellation technique. From the comprehensive simulation analysis, it can be concluded that the proposed OSPC scheme can meet the 3GPP standard requirement at different clipping ratios and it is demonstrated to outperform the conventional CPC CFR technique.

Table 3 Performance comparison of the CPC technique at different γ for three carrier signal

γ (dB)	IAR (dB) reduction at 0.01%	EVM (%)	ACLRI/ACLR2 (dBr)	CCDF at 0.1%	CCDF at 0.01%	CCDF at 0.001%
5.5	3.55	14.38	66.3/66.4	6.05	6.07	6.1
6	3.23	11.12	67.6/67.7	6.37	6.39	6.4
6.5	2.86	8.34	70.1/70.2	6.73	6.75	7.76
7	2.46	6.05	73.5/73.6	7.15	7.155	7.17

Table 4 Performance comparison of the OSPC scheme at different γ with $\delta_1 = 10$ and $\delta_2 = 3$ for three carrier signal

γ (dB)	IAR (dB) reduction at 0.01%	EVM (%)	ACLRI/ACLR2 (dBr)	CCDF at 0.1%	CCDF at 0.01%	CCDF at 0.001%
5.5	3.53	10.78	69/69.1	5.97	6.07	6.255
6	3.23	8.61	70.2/70.3	6.31	6.39	6.56
6.5	2.88	6.65	72.1/722.2	6.7	6.73	6.9
7	2.47	4.98	75.5/75.6	7.12	7.14	7.25

Acknowledgements This publication has emanated from research conducted with the financial support of Science Foundation Ireland (SFI) and is co-funded under the European Regional Development Fund under Grant Number 13/RC/2077. Pooria Varahram, Somayeh Mohammady, Ronan Farrell and John Dooley are with the Department of Electronic Engineering, National University of Ireland Maynooth (NUIM).

References

1. GPP TR 36.804 v0.7.1. (2007–2010). 3rd generation partnership project; technical specification group radio access network; evolved universal terrestrial radio access (E-UTRA); base station (BS) radio transmission and reception (release 8) (p. 185).
2. Rumney, M. (2013). *LTE and the evolution to 4G wireless*. Hoboken: Wiley.
3. Armstrong, J. (2001). New OFDM peak-to-average power ratio reduction scheme. In *IEEE 53rd vehicular technology conference* (pp. 756–760).
4. Olli, O. V., Vankka, J., & Halonen, K. (2002). *Effect of clipping in wideband CDMA system and simple algorithm for peak windowing* (pp. 614–619). San Francisco: World Wireless Congress.
5. Kim, W. J., Cho, K. J., Stapleton, S. P., & Kim, J. H. (2007). Doherty feed-forward amplifier performance using a novel crest factor reduction technique. *IEEE Microwave and Wireless Components Letter, 17*(1), 82–84.
6. Richard, V. N., & Prasad, R. (1999). *OFDM for wireless multimedia communications*. Norwood, MA: Artech House.
7. Ku, S. J. (2014). Low-complexity PTS-based schemes for PAPR reduction in SFBC MIMO–OFDM systems. *IEEE Transactions on Broadcasting, 60*(4), 650–658.
8. Yang, L., Soo, K. K., Siu, Y. M., & Li, S. Q. (2008). A low complexity selected mapping scheme by use of time domain sequence superposition technique for PAPR reduction in OFDM system. *IEEE Transactions on Broadcasting, 54*(4), 821–824.
9. Feng, G. (2015). Method and apparatus for crest factor reduction. U.S. Patent 0349994 A1.
10. Jeon, H. B., No, J. S., & Shin, D. J. (2012). A new PAPR reduction scheme using efficient peak cancellation for OFDM systems. *IEEE Transactions on Broadcasting, 58*(4), 619–628.
11. Yang, Z., Gandhi, H., Ding, I., & Jorgensen, L. (2013). Crest factor reduction for dual-band systems. In *IEEE MTT-S International Microwave Symposium Digest (IMS).* https://doi.org/10.1109/mwsym.2013.6697564.
12. Fehri, B., Boumaiza, S., & Sich, E. (2014). Crest factor reduction of inter-band multi-standard carrier aggregated signals. *IEEE Transactions on Microwave Theory and Techniques, 62*(12), 3286–3297.
13. Oppenheim, A. V., Schafer, R. W., & Buck, J. R. (1999). *Discrete-time signal processing*. Upper Saddle River, N.J: Prentice Hall.
14. Song, J., & Ochiai, H. (2016). Performance analysis for OFDM signals with peak cancellation. *IEEE Transactions on Communications, 64*(1), 261–270.
15. Huang, W. J., Hu, W. W., Li, C. P., & Chen, J. C. (2015). Novel metric-based PAPR reduction schemes for MC-CDMA systems. *IEEE Transactions on Vehicular Technology, 64*(9), 3982–3989.

16. Bahai, A. R. S., Singh, M., Goldsmith, A. J., & Saltzberg, B. R. (2002). A new approach for evaluating clipping distortion in multicarrier systems. *IEEE Journal on Selected Areas in Communications, 20*(5), 1037–1046.
17. Upton, G., & Cook, I. (2008). *A dictionary of statistics*. Oxford: OUP Oxford.
18. Liu, Q., Ma, X., Zhou, G.T., & Jie, W. (2008). Peak-to-average power ratio versus instantaneous-to-average power ratio for OFDM. In *42nd asilomar conference on signals, systems and computers* (pp. 938–942).
19. Hemphill, Ed., Summerfield, S., Wang, G., & Hawke, D. (2007). Peak cancellation crest factor reduction reference design, application note, Xilinx.

Pooria Varahram (M'10) received his B.Sc. from Khaje Nasir University of Technology in 2002, MSc degree from Tarbiat Modares University and Ph.D. from University of Putra Malaysia in Wireless Communication in 2004 and 2010, respectively. He is a senior FPGA engineer in Benetel company industrial parter with CONNECT SFI center Dublin. He was a senior postdoctoral researcher at Maynooth University from 2015 to 2017. His research interests are PAPR reduction, digital pre-distortion, and OFDM Systems.

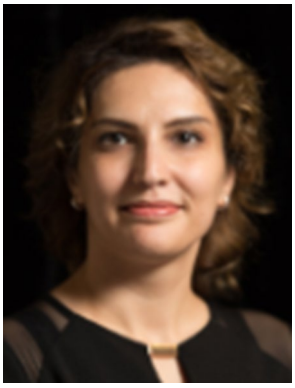

Somayeh Mohammady (M'06) received her B.Sc. of Electronic Engineering from Azad University of Naein in 2005, M.Sc. and Ph.D. degrees from University Putra Malaysia (UPM) in Electronic Engineering in 2008 and 2012, respectively. She is a Lecturer in school of Electrical and Electronic Engineering at Technological University Dublin (TU Dublin), she is an Associate Investigator with CONNECT Trinity College, Dublin, Ireland. Her research areas are Digital Signal Processing and Efficiency Improvement algorithms in OFDM based systems, Automations, Robotics, and Integration of Internet of things (IoT) and 5G NR.

Ronan Farrell (S'95-M'98) received his B.E. and Ph.D. degrees in electronic engineering from University College Dublin, Ireland, in 1993 and 1998, respectively. Ronan is currently Dean of the Faculty of Science and Engineering, and a Professor in the Department of Electronic Engineering at Maynooth University, Ireland. His research interests include physical layer communication technologies, in particular, adaptive receivers, PAs and active antenna arrays. He is currently the strand leader responsible for radio technologies in the SFI-funded CONNECT Centre for the Internet of Things.

John Dooley (M'08) was born in Dublin, Ireland. He received the B.E. degree in Electronic Engineering and the Ph.D. degree in Microwave Engineering from University College Dublin, Ireland in 2001 and 2008, respectively. From 2008, he has been a Postdoctoral Research Fellow in National University of Ireland Maynooth, Department of Electronic Engineering. He is currently a lecturer in wireless communications at Maynooth University. His current research interests are nonlinear analysis and digital techniques applied to wireless communications, active antenna arrays, massive MIMO and digital pre-distortion.